New calculations of gross β-decay properties for astrophysical applications $\Rightarrow$ "Speeding-up the classical r-process"

Peter Möller
Theoretical Division, Los Alamos National Laboratory, Los Alamos, NM 87545

Bernd Pfeiffer and Karl-Ludwig Kratz
Institut für Kernchemie, Universität Mainz, Germany

May 22, 2002

Abstract: Recent compilations of experimental gross β-decay properties, i.e. half-lives ($T_{1/2}$) and neutron-emission probabilities ($P_{\rm n}$), are compared to improved global macroscopic-microscopic model predictions. The model combines calculations within the quasi-particle random-phase approximation (QRPA) for the Gamow-Teller (GT) part, with an empirical spreading of the QP-strength, and the gross theory for the first-forbidden (*ff*) part of β^--decay. Nuclear masses are either taken from the recent Audi et al. data compilation, when available, or from the finite-range droplet model (FRDM). In particular for spherical and neutron-(sub-)magic isotopes, a considerable improvement compared to our earlier predictions for pure GT-decay [ADNDT 1997] is observed. $T_{1/2}$ and $P_{\rm n}$ values up to the neutron drip-line have been applied to r-process calculations within the classical "waiting-point" approximation. With the new nuclear-physics input, a considerable speeding-up of the r-matter flow is observed, in particular at the r-abundance peaks which are related to magic neutron-shell closures.

1 Introduction

Interactions between astrophysics and nuclear physics have been longstanding and rewarding. To the nuclear physicist many phenomena in the universe represent nuclear experiments on a grand scale, often under conditions that cannot be replicated on earth. To the astrophysicist nuclear physics represents experimental and theoretical sources of data which are needed to model the energy balances and time scales in many astrophysical scenarios. Examples of this dichotomy are the explanation of the source of the energy production in the sun and the postulation of a rapid-neutron-capture process, or r-process [1] as the origin of many heavy nuclei beyond Fe.

To us, modeling the r-process has represented a particularly fascinating challenge. Its detailed study requires input of nuclear data from experiment and/or theory. However, properly designed studies can also provide information to the nuclear theorist on nuclear properties far from stability that are inaccessible to experimental study. Informative studies of the r-process can be accomplished with a knowledge of just a few nuclear properties, namely the nuclear mass, from which neutron separation energies $S_{\rm n}$ and β-decay Q_β values can trivially be obtained, the β-decay half-lives $T_{1/2}$, and β-delayed neutron-emission probabilities $P_{\nu{\rm n}}$. More elaborate studies require additional quantities for example reaction rates and temperature dependences of many quantities.

A great leap forward in our understanding of the r-process and other stellar nucleo-synthesis processes took place about 10 years ago when data from global, unified, microscopic nuclear-structure models for the nuclear mass and β-decay were used for the first time in such calculations [2]. A key new feature was the reliability of the nuclear-structure models also outside the regions where the model parameters were determined that is for regions of neutron-rich nuclei beyond the experimentally known region near β-stability. Most influential in the first studies of this type were the "Möller–Nix" mass models and the "Krumlinde–Möller–Randrup" Quasi-Particle Random-Phase (QRPA) model of β-decay. The first "Möller-Nix" mass model was published in 1981 [3]; its current enhanced form (FRDM (1992)) was finalized in 1992 and published in 1995 [4]. The initial QRPA model is from 1984 [5] with numerous enhancements added over the next several years. An extensive discussion of the enhanced model was published in 1990 [6]. Tabulated β-decay properties for 8979 nuclei from ^{16}O and beyond appeared in 1997 [7].

There are only a very few realistic mass models in which microscopic effects are calculated from microscopic effective interactions. Single-particle potentials in the macroscopic-microscopic approach and two-body Skyrme-type potentials in Hartree-Fock models are two examples of such "microscopic" interactions. Calculations based on such potentials are, apart from the work mentioned above, for example the early work by Seeger and Howard [8] in a macroscopic-microscopic approach and more current work based on Skyrme interactions [9–11] All these mass models have an rms error of about 0.7 MeV in the region where the model constants were adjusted, and do not diverge, so far, outside the region of adjustment, that is when new masses are measured and compared to published masses the rms error is still about 0.7 MeV. Despite such errors much has been learned about the r-process from calculations based on these nuclear data sources.

It is noteworthy that for 20 years the error of the realistic, extrapolatable mass models has remained fairly constant at about 0.7 MeV (our 1981 mass model error was 0.835 MeV). Very recently we have even seen results of the first self-consistent HF mass model with two-body Skyrme-type forces with optimized parameters. Also in this approach the mass model rms error is near 0.7 MeV. A recent analysis by Bohigas and Lebœuf [12, 13] proposes that this empirically observed lower limit that seems almost like a brick wall that is impossible to surmount is actually obtained as a lower limit for the error for models of this type from very general and fundamental arguments. Because of correlations in the mass errors for nuclei close to each other in the

nuclear chart, this translates to about ±0.5 MeV errors in calculated Q_β and S_n values. It may therefore be very difficult to develop a mass model that is not subject to these limitations. In our efforts to improve the nuclear data input of our astrophysical r-process calculations we will therefore in our new studies here focus less on the mass models and the masses they produce, which directly relates to the *structure* of the r-abundances and instead concentrate more on the β-decay models from which we obtain decay half-lives that relate directly to the *time-scale* of the r-process. However, due to correlations of Q_β and S_n errors with calculated β-decay properties again for nuclei far from stability $T_{1/2}$ and P_n values can only be predicted within about a factor 2 to 3. We will therefore present some highlights of the 1990 version of our β-decay model and then introduce and justify two enhancements to this model. We then study the consequences of the model improvements in r-process calculations.

2 Models

Theoretically, the two integral β-decay quantities, $T_{1/2}$ and P_n, are interrelated via their usual definition in terms of the so-called β-strength function ($S_\beta(E)$) [14]:

$$1/T_{1/2} = \sum_{0 \le E_i \le Q_\beta} S_\beta(E_i) \times f(Z, R, Q_\beta - E_i); \tag{1}$$

where R is the nuclear radius, Q_β is the maximum β-decay energy (or the isobaric mass difference) and $f(Z, R, Q_\beta - E_i)$ the Fermi function. With this definition, $T_{1/2}$ may yield information on the *average* β-feeding of a nucleus. However, since the low-energy part of its excitation spectrum is strongly weighted by the energy factor of β-decay, $f \sim (Q_\beta - E_i)^5$, $T_{1/2}$ is dominated by the lowest-energy resonances in $S_\beta(E_i)$; i.e. by the (near-) ground-state allowed GT or *ff* transitions.

The β-delayed neutron emission probability (P_n) is schematically given by

$$P_\mathrm{n} = \frac{\sum_{B_\mathrm{n}}^{Q_\beta} S_\beta(E_i) f(Z, R, Q_\beta - E_i)}{\sum_{0}^{Q_\beta} S_\beta(E_i) f(Z, R, Q_\beta - E_i)} \tag{2}$$

thus defining P_n as the ratio of the integral β-intensity to states above the neutron separation energy S_n to the total β-intensity. As done in nearly all P_n calculations, in the above equation, the ratio of the partial widths for l-wave neutron emission ($\Gamma^j_\mathrm{n}(E_\mathrm{n})$) and the total width ($\Gamma_\mathrm{tot} = \Gamma^j_\mathrm{n}(E_\mathrm{n}) + \Gamma_\gamma$) is set equal to 1; i.e. possible γ-decay from neutron-unbound levels is neglected. Again, because of the $(Q_\beta - E)^5$ dependence of the Fermi function, the physical significance of the P_n quantity is limited, too. It mainly reflects the β-feeding to the energy region just beyond S_n. Taken together, however, the two gross decay properties, $T_{1/2}$ **and** P_n, may well provide some first information about the nuclear structure determining β-decay. Generally speaking, for a given Q_β value a *short* half-life usually correlates with a *small* P_n value, and vice versa. This is actually more than a simple rule of thumb; it can be used to check the consistency of experimental numbers. Sometimes even global plots of double-ratios of experimental to theoretical P_n to $T_{1/2}$ relations are used to show systematic trends, see for example Ref. [15]. Several impressive examples in literature show that it is sometimes possible to identify special nuclear-structure features solely from $T_{1/2}$ and P_n. Among them are: (i) the development of single-particle (SP) structures and related ground-state shape changes in the $50 \le N \le 60$ region of the Sr isotopes [5, 16], (ii) the at that time totally unexpected prediction of collectivity of neutron-magic (N=28) ^{44}S situated two proton-pairs below the doubly-magic ^{48}Ca [17], and (iii) the very recent interpretation of the surprising decay properties of ^{131,132}Cd just above $N = 82$ [18–20].

Today, in studies of nuclear-structure features, even of gross properties such as the $T_{1/2}$ and $P_{\rm n}$ values considered here, a substantial number of different theoretical approaches are used. The significance and sophistication of these models and their relation to each other should, however, be clear before they are applied. In general, one can assign the nuclear models used to calculate the above two decay properties to the following different groups:

1. *Models where the physical quantity of interest is given by an expression such as a polynomial or an algebraic expression.*
   Normally, the parameters are determined by adjustments to experimental data and describe only a single nuclear property. No nuclear wave functions are obtained in these models. Examples of theories of this type are purely empirical approaches that assume a specific shape of S_β(E) (either constant or proportional to level density), such as the Kratz-Herrmann formula [21] or the statistical gross theory of β-decay [22, 23] These models can be considered to be analogous to the liquid-drop model of nuclear masses, and are —again— appropriate for dealing with *average* properties of β-decay, however taking into account the Ikeda sum-rule to quantitatively define the total strength. In both types of approaches, model-inherently no insight into the underlying single-particle (SP) structure is possible.

2. *Models that use an effective nuclear interaction and usually solve the microscopic quantum-mechanical Schrödinger or Dirac equation.*
   The approaches that actually solve the Schrödinger equation provide nuclear wave functions which allow a variety of nuclear properties (e.g. ground-state shapes, level energies, spins and parities, transition rates, $T_{1/2}$, $P_{\nu \rm n}$, etc.) to be modeled within a single framework. Most theories of this type that are currently used in large-scale calculations, such as e.g. the FRDM+QRPA model [7] used here or the ETFSI+cQRPA approach [9, 24], in principle fall into two subgroups, depending on the type of microscopic interaction used. Another aspect of these models is, whether they are restricted to spherical shapes, or to even-even isotopes, or whether they can describe **all** nuclear shapes and **all** types of nuclei:

   (a) SP approaches that use a simple central potential with additional residual interactions. The Schrödinger equation is solved in a SP approximation and additional two-body interactions are treated in the BCS, Lipkin-Nogami, or RPA approximations, for example. To obtain the nuclear potential energy as a function of shape, one combines the SP model with a macroscopic model, which then leads to the macroscopic-microscopic model. Within this approach, the nuclear ground-state energy is calculated as a sum of a microscopic correction obtained from the SP levels by use of the Strutinsky method and a macroscopic energy.

   (b) Hartree-Fock-type models, in which the postulated effective interaction is of a two-body type. If the microscopic Schrödinger equation is solved then the wave functions obtained are anti-symmetrized Slater determinants. In such models, it is possible to obtain the nuclear ground-state energy as $E =< \Psi_0|H|\Psi_0 >$, otherwise the HF have many similarities to those in category 2a but have fewer parameters.

In principle, models in group 2b are expected to be more accurate, because the wave functions and effective interactions can in principle be more realistic. However, two problems still remain today: what effective interaction is sufficiently realistic to yield more accurate results, and what are the optimized parameter values for such a two-body interaction?

Some models in category 2 have been overparameterized, which means that their microscopic origins have been lost and the results are just parameterizations of the experimental data. Examples of such models are the calculations Refs. [25, 26], where the strength of the residual GT interaction has been fitted for each element (Z-number) in order to obtain optimum reproduction of known $T_{1/2}$ and $P_{\rm n}$ values in each isotopic chain.

To conclude this section, let us emphasize that there is no "correct" model in nuclear physics. Any modeling of nuclear-structure properties involves approximations of the true forces and equations with the goal to obtain a formulation that can be solved in practice, but that "retains the essential features" of the true system under study, so that one can still learn something. What we mean by this, depends on the actual circumstances. It may well turn out that when proceeding from a simplistic, macroscopic approach to a more microscopic model, the first overall result may be "worse" just in terms of agreement between calculated and measured data. However, the disagreements may now be understood more easily, and further nuclear-structure-based, realistic improvements will become possible.

3 Prediction of $T_{1/2}$ and $P_{\rm n}$ values from FRDM-QRPA

The formalism we use to calculate Gamow-Teller (GT) β-strength functions is fairly lengthy since it involves adding pairing and Gamow-Teller residual interactions to the folded-Yukawa single-particle Hamiltonian and solving the resulting Schrödinger equation in the quasi-particle random-phase approximation (QRPA). Because this model has been completely described in two previous papers [5, 6] we refer to those two publications for a full model specification and for a definition of notation used. We restrict the discussion here to an overview of features that are particularly relevant to the results discussed in this paper.

It is well known that wave functions and transition matrix elements are more affected by small perturbations to the Hamiltonian than are the eigenvalues. When transition rates are calculated it is therefore necessary to add residual interactions to the folded-Yukawa single-particle Hamiltonian in addition to the pairing interaction that is included in the mass model. Fortunately, the residual interaction may be restricted to a term specific to the particular type of decay considered. To obtain reasonably accurate half-lives it is also very important to include ground-state deformations. Originally the QRPA formalism was developed for and applied only to spherical nuclei [27, 28] The extension to deformed nuclei, which is necessary in global calculations of β-decay properties, was first described in 1984 [5]. To treat Gamow-Teller β-decay we therefore add the Gamow-Teller force

$$V_{\rm GT} = 2\chi_{\rm GT} : \boldsymbol{\beta^{1-}} \cdot \boldsymbol{\beta^{1+}} : \tag{3}$$

to the folded-Yukawa single-particle Hamiltonian, after pairing has already been incorporated, with the standard choice $\chi_{\rm GT} = 23$ MeV$/A$ [5, 6, 27, 28]. Here $\boldsymbol{\beta^{1\pm}} = \sum_i \boldsymbol{\sigma_i} \boldsymbol{t_i^{\pm}}$ are the Gamow-Teller $\beta^{\pm}$-transition operators.

The process of β decay occurs from an initial ground state or excited state in a mother nucleus to a final state in the daughter nucleus. For β^- decay, the final configuration is a nucleus in some excited state or its ground state, an electron (with energy $E_{\rm e}$), and an anti-neutrino (with energy E_ν). The decay rate w_{fi} to one nuclear state f is

$$w_{fi} = \frac{m_0 c^2}{\hbar} \frac{\Gamma^2}{2\pi^3} |M_{fi}|^2 f(Z, R, \epsilon_0) \tag{4}$$

where R is the nuclear radius and $\epsilon_0 = E_0/m_0c^2$, with m_0 the electron mass. Moreover, $|M_{fi}|^2$ is the nuclear matrix element, which is also the β-strength function. The dimensionless constant

Γ is defined by

$$\Gamma \equiv \frac{g}{m_0 c^2}\left(\frac{m_0 c}{\hbar}\right)^3 \tag{5}$$

where g is the Gamow-Teller coupling constant. The quantity $f(Z,R,\epsilon_0)$ has been extensively discussed and tabulated elsewhere [29–31]

For the special case in which the two-neutron separation energy $S_{2\mathrm{n}}$ in the daughter nucleus is greater than Q_β, the energy released in ground-state to ground-state β decay, the probability for β-delayed one-neutron emission, in percent, is given by

$$P_{1\mathrm{n}} = 100\,\frac{\sum\limits_{S_{1\mathrm{n}}<E_f<Q_\beta} w_{fi}}{\sum\limits_{0<E_f<Q_\beta} w_{fi}} \tag{6}$$

where $E_f = Q_\beta - E_0$ is the excitation energy in the daughter nucleus and $S_{1\mathrm{n}}$ is the one-neutron separation energy in the daughter nucleus. We assume that decays to energies above $S_{1\mathrm{n}}$ always lead to delayed neutron emission.

To obtain the half-life with respect to β decay one sums up the decay rates w_{fi} to the individual nuclear states in the allowed energy window. The half-life is then related to the total decay rate by

$$T_\beta = \frac{\ln 2}{\sum\limits_{0<E_f<Q_\beta} w_{fi}} \tag{7}$$

The above equation may be rewritten as

$$T_\beta = \frac{\hbar}{m_0 c^2}\,\frac{2\pi^3 \ln 2}{\Gamma^2}\,\frac{1}{\sum\limits_{0<E_f<Q_\beta} |M_{fi}|^2 f(Z,R,\epsilon_0)} = \frac{B}{\sum\limits_{0<E_f<Q_\beta} |M_{fi}|^2 f(Z,R,\epsilon_0)} \tag{8}$$

with

$$B = \frac{\hbar}{m_0 c^2}\,\frac{2\pi^3 \ln 2}{\Gamma^2} \tag{9}$$

For the value of B corresponding to Gamow-Teller decay we use [5, 6]

$$B = 4131 \text{ s} \tag{10}$$

The energy released in ground-state to ground-state electron decay is given in terms of the atomic mass excess $M(Z,N)$ or the total binding energy $E_{\mathrm{bind}}(Z,N)$ by

$$Q_{\beta^-} = M(Z,N) - M(Z+1,N-1) \tag{11}$$

The above formulas apply to the β^- decays that are of interest here. The decay Q values and neutron separation energies $S_{\nu\mathrm{n}}$ are obtained from our FRDM mass model when experimental data are unavailable [4]. The matrix elements M_{fi} are obtained from our QRPA model. More details are provided elsewhere [6].

We compare here two calculations. The first is our original model as described in Ref. [6] with the following enhancements:

1. To calculate β-decay Q-values and neutron separation energies $S_{\nu\mathrm{n}}$ we use experimental ground-state masses where available, otherwise calculated masses [4]. In our previous recent calculations we used the 1989 mass evaluation [32]; here we use the 1995 mass evaluation [33].

2. It is known that at higher excitation energies additional residual interactions result in a spreading of the transition strength. In our 1997 calculation each transition goes to a precise, well-specified energy in the daughter nucleus. This can result in very large changes in the calculated $P_{\rm n}$ values for minute changes in, for example $S_{1\rm n}$, depending on whether an intense, sharp transition is located just below or just above the neutron separation energy [6]. To remove this unphysical feature we introduce an empirical spreading width that sets in above 2 MeV. Specifically, each transition strength "spike" above 2 MeV is transformed to a Gaussian of width

$$\Delta_{\rm sw} = \frac{8.62}{A^{0.57}} \tag{12}$$

   This choice is equal to the error in the mass model. Thus, it accounts approximately for the uncertainty in calculated neutron separation energies and at the same time it roughly corresponds to the observed spreading of transition strengths in the energy range 2–10 MeV, which is the range of interest here.

3. We also base our calculations on more correct ground-state deformations which affect the energy levels and wave-functions that are obtained in the single-particle model. The ground-state deformations calculated in the FRDM mass model (Möller *et al.*, 1992), generally agree with experimental observations, but in transition regions between spherical and deformed nuclei discrepancies do occur. We therefore replace calculated deformations with spherical shape, when experimental data so indicate. This has been done for the following local regions:

   (i) in the Fe-group seed region at the $N = 40$ sub-shell closure

   (ii) for $31 < Z < 39$, $52 < N < 60$ isotopes and

   (iii) for $51 < Z < 55$, $84 < N < 90$ nuclides.

In the second approach we account for the effect of first-forbidden strength, calculated in the statistical gross theory [22, 23], on the decay half-lives and β-delayed neutron-emission probabilities. Relative to the allowed Gamow-Teller strength which over a given energy range is represented by relatively few strong peaks, the first forbidden strength with its numerous small, densely spaced, peaks to a good approximation constitutes a "smooth background". It is therefore a reasonable approach to calculate the GT transitions in a microscopic QRPA approach and the *ff* transitions in a macroscopic statistical model, in analogy with the macroscopic-microscopic method in which the nuclear energy as a function of shape is calculated as a sum of a liquid-drop-type model that varies smoothly with proton number, neutron number, and deformation and a shell-correction part that exhibits rapid variation in these variables. Strictly speaking $f(Z, R, \epsilon_0)$ is different for allowed and first forbidden transitions. Here we use the same $f(Z, R, \epsilon_0)$ in both cases, a negligible approximation in our statistical model of the first forbidden decays.

We show in Figs. 1–3 the effect of two of our model enhancements on the strength functions, half-lives and delayed neutron probabilities for ^{99}Rb, ^{92}Rb and ^{137}I. The top subplot shows the original model, the middle subplot the effect of spreading the transition strength, and the bottom subplot the effect of also including *ff* transitions.

The first case, ^{99}Rb in Fig. 1, is a well deformed nucleus. In the original model there is significant strength at low energies as is often the case in deformed nuclei. Therefore there is for this nucleus little effect of our two model enhancements: strength spreading and inclusion of *ff* transitions. In contrast, for the spherical ^{92}Rb nucleus shown in Fig. 2 and for ^{137}I in Fig. 3 the effect of the two improvements is dramatic. We have chosen ^{92}Rb as one illustrative

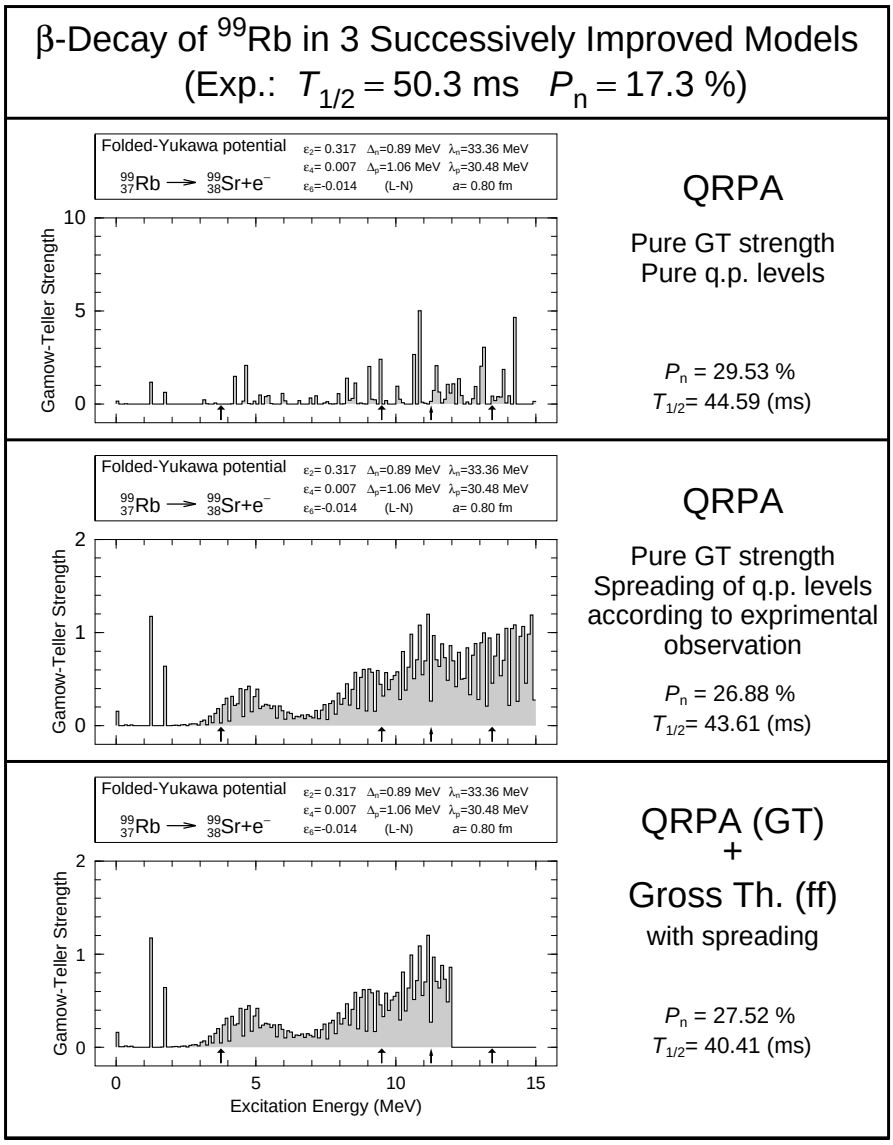

Figure 1: Calculated β-strength functions, corresponding half-lives and delayed-neutron emission probabilities for ^{99}Rb in three successively enhanced models. The narrow arrow indicates the Q_β value, the wide arrows successive neutron-separation energies; the lowest arrow $S_{1\mathrm{n}}$, the second lowest $S_{2\mathrm{n}}$, and so on. The results are further discussed in the text.

example for two reasons. First, in the standard model calculation illustrated in the top subplot $S_{1\mathrm{n}}$ sits just below the first major peak in the strength function, with some strength, not discernable on this plot occurring below the one-neutron separation energy. This leads to a very high delayed-neutron emission probability, in contradiction to experiment. Second, most of the strength occurring within the Q_β window lies *just below* Q_β. Therefore we obtain a half-life in the order of hours, again in contradiction with experiment. Already after implementing the first model enhancement, the spreading of the GT strength the agreement with experiment improves considerably: the half-life is reduced by a factor of 6.5 and the delayed-neutron emission probability by a factor of 20! In the next step there are even more dramatic changes in the calculated half-life and neutron-emission probability and the agreement with experiment is now quite good. The last case, ^{137}I, has been chosen as a typical example in the heavy fission-peak

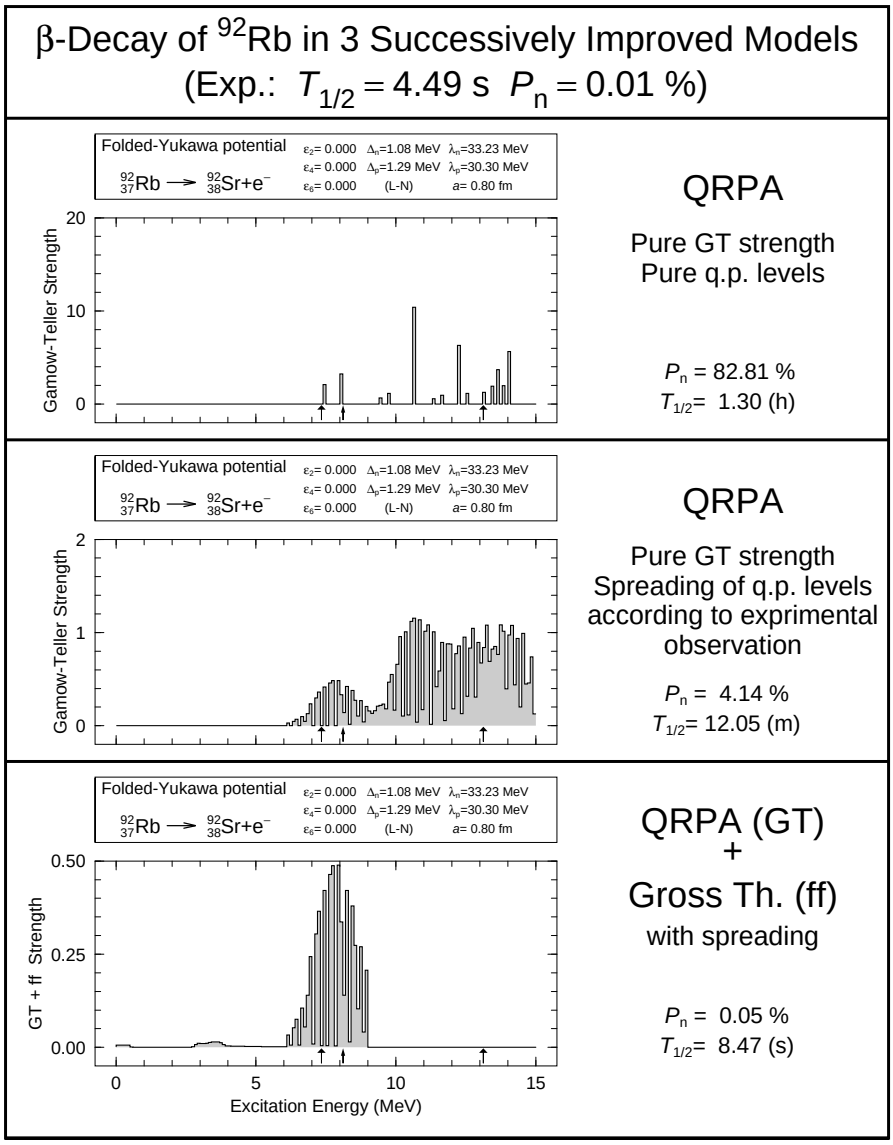

Figure 2: Calculated β-strength functions, corresponding half-lives and delayed-neutron emission probabilities for ^{92}Rb in three successively enhanced models. The narrow arrow indicates the Q_β value, the wide arrows successive neutron-separation energies; the lowest arrow $S_{1\mathrm{n}}$, the second lowest $S_{2\mathrm{n}}$, and so on. The results are further discussed in the text.

mass region where – consistently – there is no low-lying GT strength. In the initial model there are large differences between the calculated and experimental $T_{1/2}$ and P_n values. The effect of the spreading of the GT strength is somewhat less dramatic than for ^{92}Rb but after the *ff* strength is included we again achieve good agreement with experimental data.

It is not our aim here to make a detailed analysis of each individual nucleus, but instead to present an overview of the model performance in a calculation of a large number of β-decay half-lives and delayed neutron-emission probabilities. In Figs. 4 and 5 we compare measured β^--decay half-lives and β-delayed neutron-emission probabilities with calculations based on our two models, for nuclei throughout the periodic system. To address the reliability versus distance from stability, we present the ratio $T_{\beta,\mathrm{calc}}/T_{\beta,\mathrm{exp}}$ versus the quantity $T_{\beta,\mathrm{exp}}$. Because the relative error in the calculated half-lives is more sensitive to small shifts in the positions of the calculated

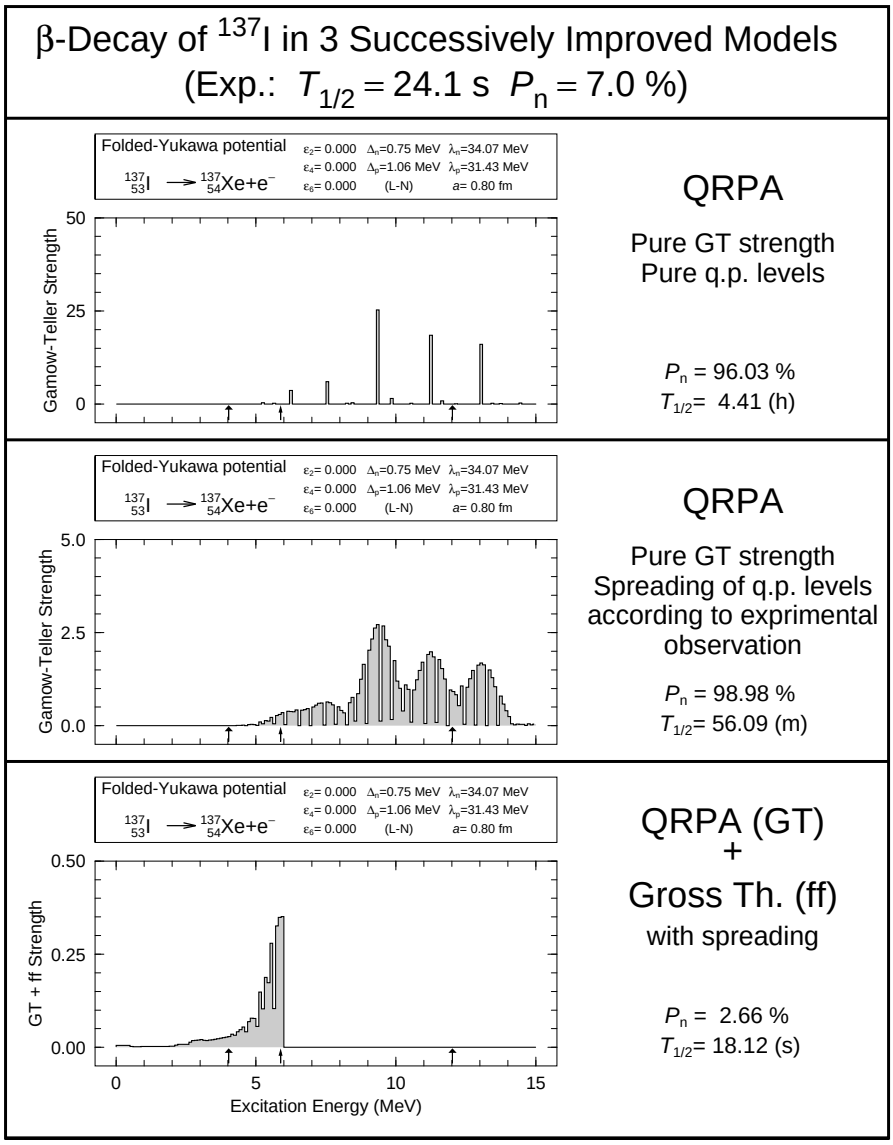

Figure 3: Calculated β-strength functions, corresponding half-lives and delayed-neutron emission probabilities for ^{137}I in three successively enhanced models. The narrow arrow indicates the Q_β value, the wide arrows successive neutron-separation energies; the lowest arrow S_{1n}, the second lowest S_{2n}, and so on. The results are further discussed in the text.

single-particle levels for decays with small energy releases, where long half-lives are expected, one can anticipate that half-life calculations are more reliable far from stability, where the β-decay Q-values are large, than close to β-stable nuclei.

Before we make a quantitative analysis of the agreement between calculated and experimental half-lives we briefly discuss what conclusions can be drawn from a simple visual inspection of Fig. 4. As functions of $T_{\beta,\mathrm{exp}}$ one would expect the average error to increase as $T_{\beta,\mathrm{exp}}$ increases. This is indeed the case in both of the model calculations. When, as in the lower part of the figure, *ff* transitions are included the agreement between calculations and experiment is better, in particular for long half-lives, as expected, because for the small decay Q values here the *ff* transitions are relatively more important. In addition one is left with the impression that the errors in our calculation are fairly large. However, this is partly a fallacy, since for small

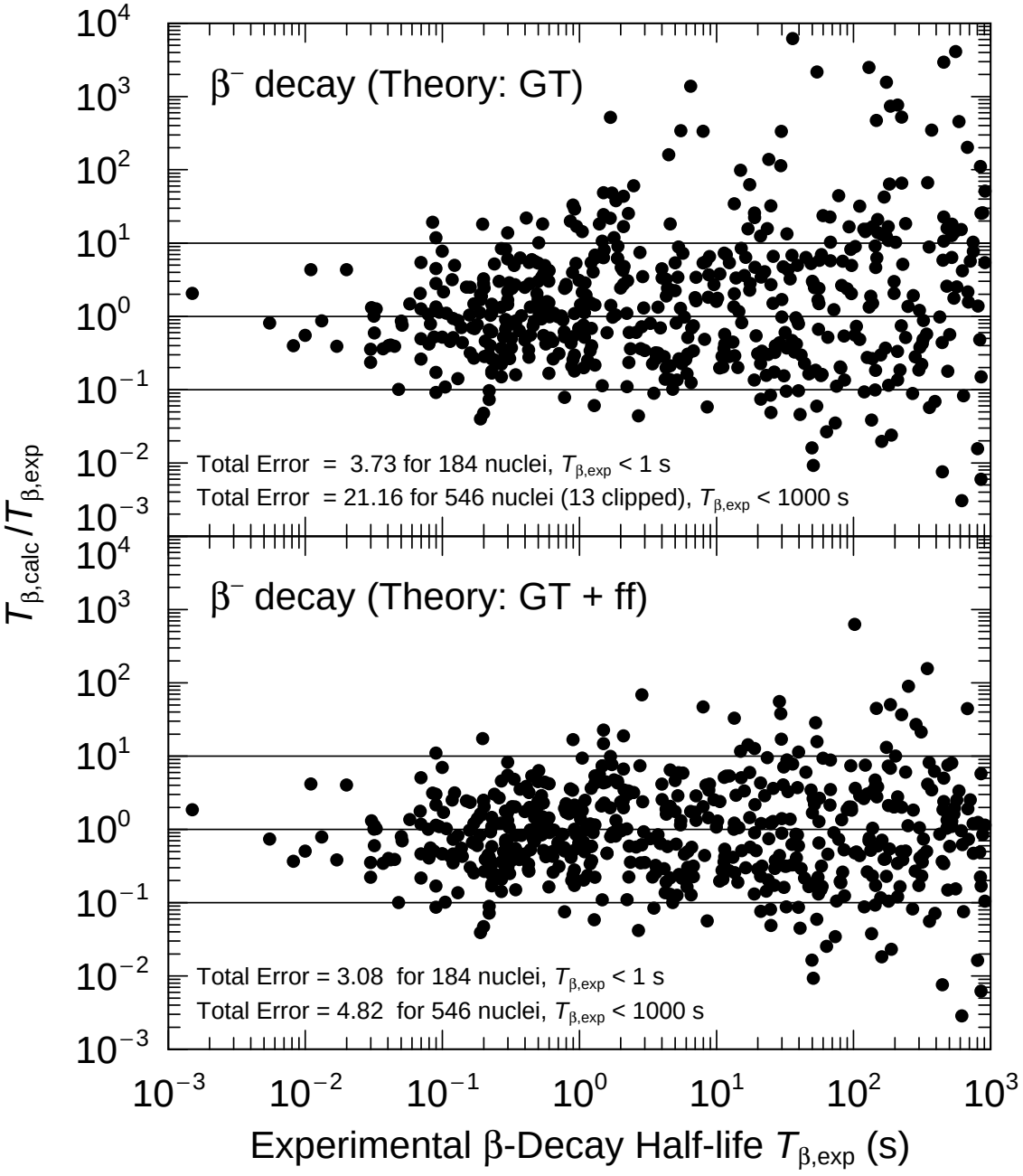

Figure 4: Ratio of calculated to experimental β^--decay half-lives for nuclei from ^{16}O to the heaviest known in our previous and current models.

errors there are many more points than for large errors. This is not clearly seen in the figures, since for small errors many points are superimposed on one another. To obtain a more exact understanding of the error in the calculation we therefore perform a more detailed analysis.

One often analyzes the error in a calculation by studying a root-mean-square (rms) deviation, which in this case would be

$$\sigma_{\rm rms}{}^2 = \frac{1}{n}\sum_{i=1}^{n}(T_{\beta,\rm exp} - T_{\beta,\rm calc})^2 \tag{13}$$

However, such an error analysis is unsuitable here, for two reasons. First, the quantities studied

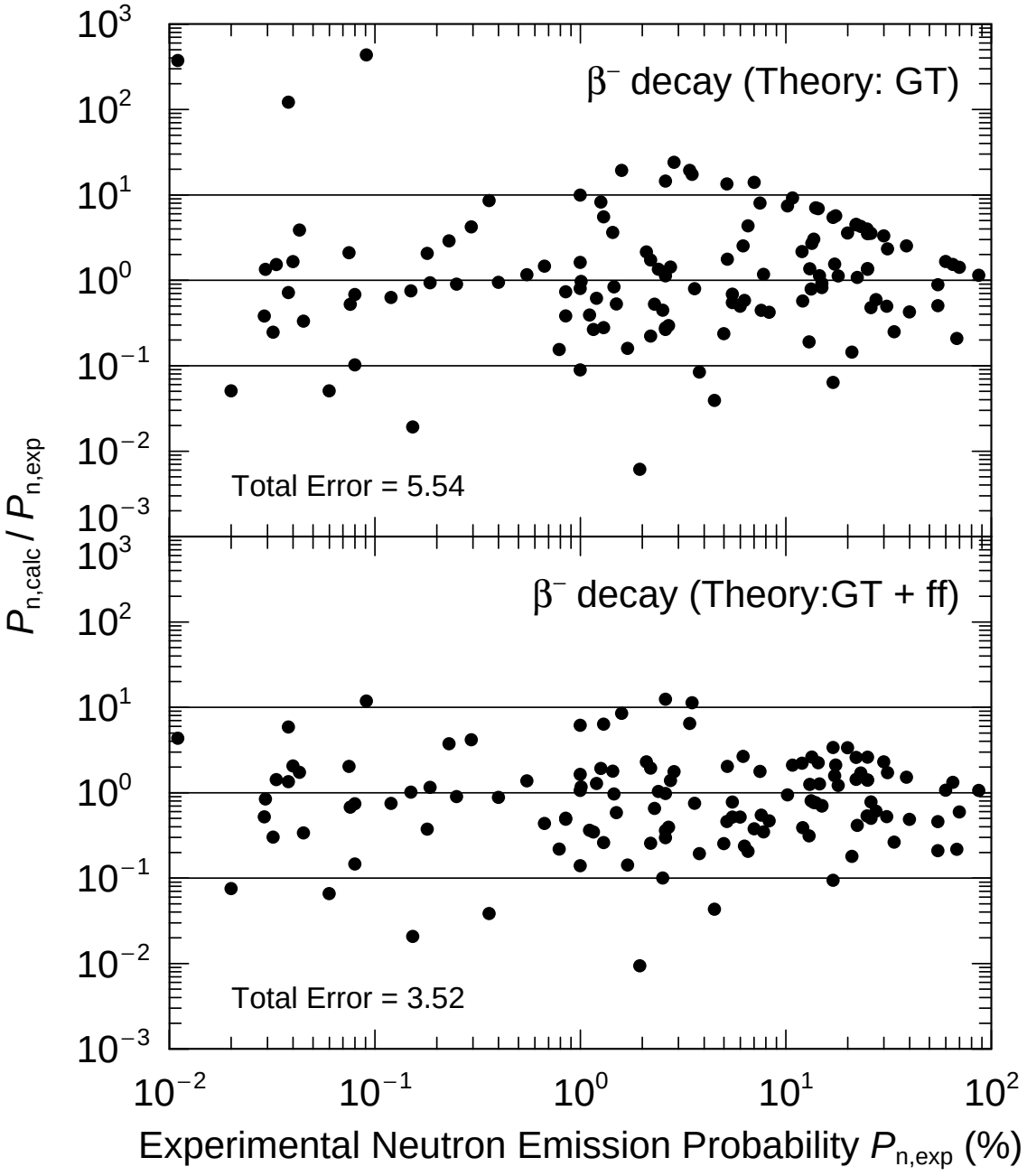

Figure 5: Ratio of calculated to experimental β-delayed neutron-emission probabilities $P_{\rm n}$ for nuclei in the fission-fragment region in our previous and current models.

vary by many orders of magnitude. Second, the calculated and measured quantities may *differ* by orders of magnitude. We therefore study the quantity $\log(T_{\beta,\rm calc}/T_{\beta,\rm exp})$, which is plotted in Fig. 4, instead of $(T_{\beta,\rm exp} - T_{\beta,\rm calc})^2$. We present the formalism here for the half-life, but the formalism is also used to study the error of our calculated $P_{\rm n}$ values.

To facilitate the interpretation of the error plots we consider two hypothetical cases. As the first example, suppose that all the points were grouped on the line $T_{\beta,\rm calc}/T_{\beta,\rm exp} = 10$. It is immediately clear that an error of this type could be entirely removed by introducing a renormalization factor, which is a common practice in the calculation of β-decay half-lives. We

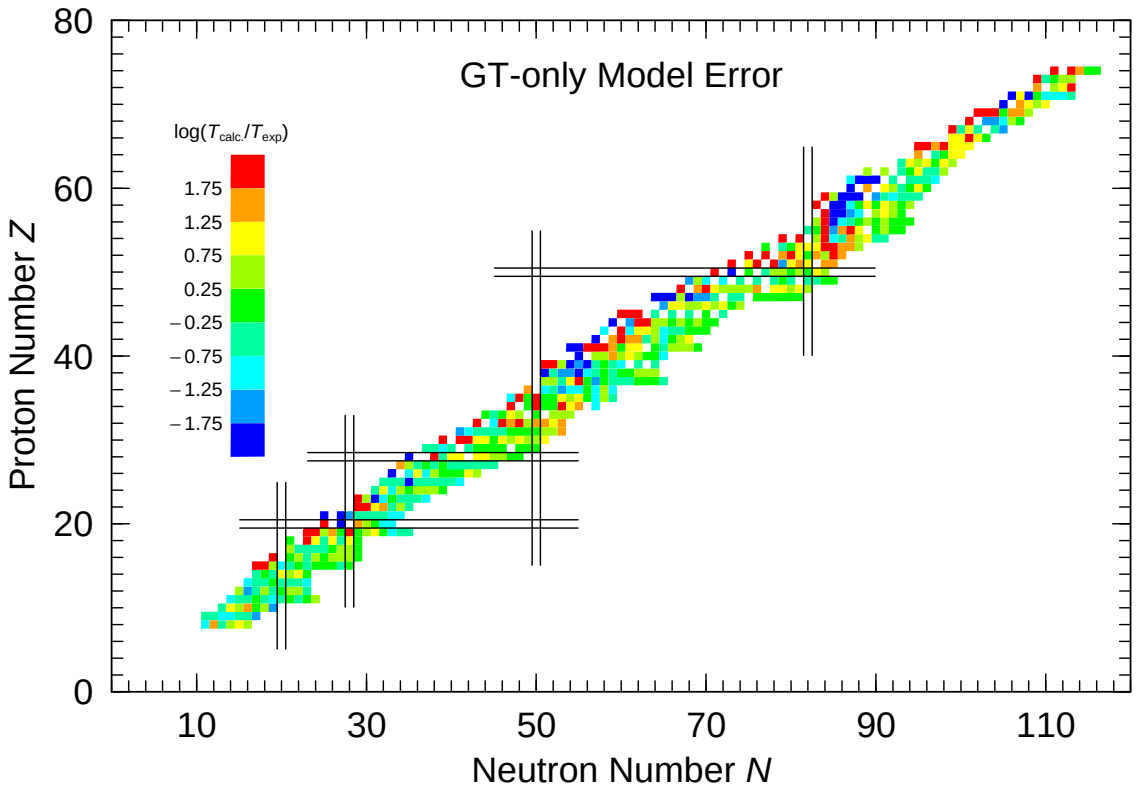

Figure 6: "Nuclear-chart" plot of the ratio of calculated to experimental β^--decay half-lives for nuclei from ^{16}O to the heaviest known.

shall see below that in our model the half-lives corresponding to our calculated strength functions have about zero average deviation from the calculated half-lives, so no renormalization factor is necessary.

In another extreme, suppose half the points were located on the line $T_{\beta,\mathrm{calc}}/T_{\beta,\mathrm{exp}} = 10$ and the other half on the line $T_{\beta,\mathrm{calc}}/T_{\beta,\mathrm{exp}} = 0.1$. In this case the average of $\log(T_{\beta,\mathrm{calc}}/T_{\beta,\mathrm{exp}})$ would be zero. We are therefore led to the conclusion that there are several types of errors that are of interest to study, namely the average position of the points in Fig. 4, which is just the average of the quantity $\log(T_{\beta,\mathrm{calc}}/T_{\beta,\mathrm{exp}})$, and the spread of the points around this average. To analyze the error along these ideas, we introduce the quantities

$$\begin{aligned}
r &= T_{\beta,\mathrm{calc}}/T_{\beta,\mathrm{exp}} \\
r_1 &= \log_{10}(r) \\
M_{r_1} &= \tfrac{1}{n}\textstyle\sum_{i=1}^{n} r_1^i \\
M_{r_1}^{10} &= 10^{M_{r_1}} && \text{Mean Deviation (Factor)} \\
\sigma_{r_1} &= \left[\tfrac{1}{n}\textstyle\sum_{i=1}^{n}\left(r_1^i - M_{r_1}\right)^2\right]^{1/2} \\
\sigma_{r_1}^{10} &= 10^{\sigma_{r_1}} && \text{Mean Fluctuation (Factor)} \\
\Sigma_{r_1} &= \left[\tfrac{1}{n}\textstyle\sum_{i=1}^{n}\left(r_1^i\right)^2\right]^{1/2} \\
\Sigma_{r_1}^{10} &= 10^{\Sigma_{r_1}} && \text{Total Error (Factor)}
\end{aligned} \tag{14}$$

where M_{r_1} is the average position of the points and σ_{r_1} is the spread around this average. When we prefer to represent the error by a single number we use the measure $\Sigma_{r_1}^{10}$ for the "Total"

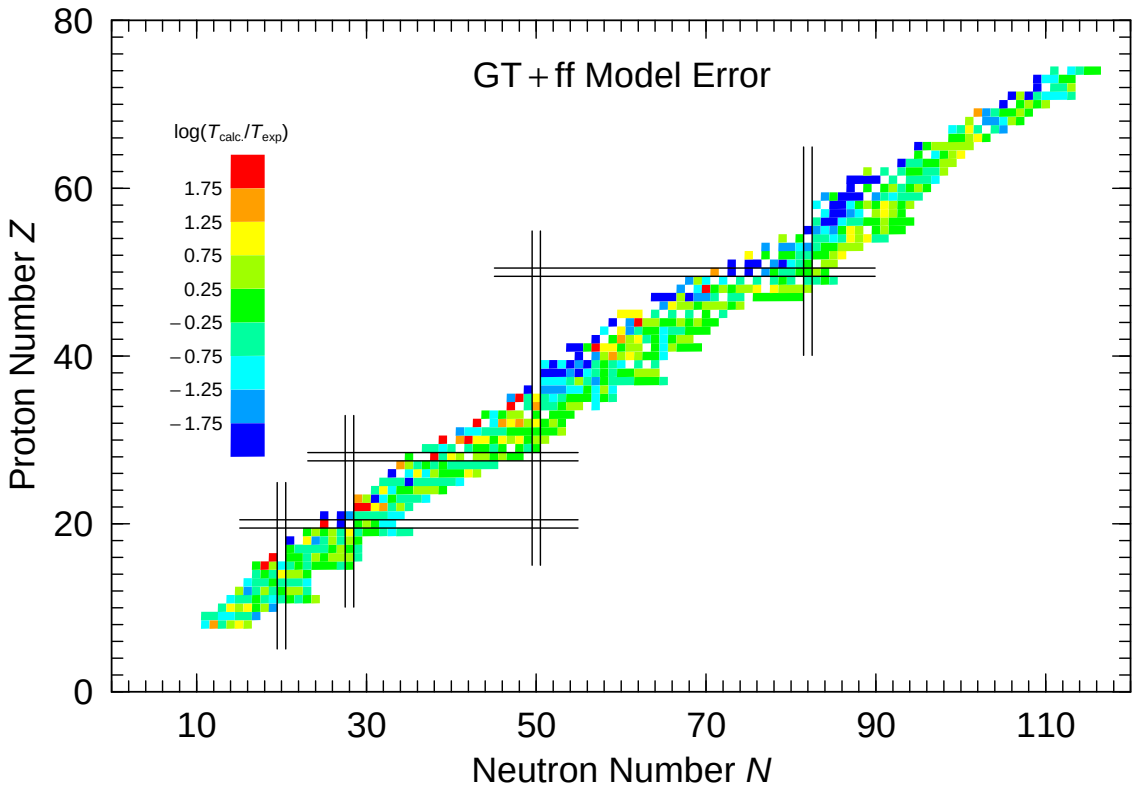

Figure 7: "Nuclear-chart" plot of the ratio of calculated to experimental β^--decay half-lives for nuclei from ^{16}O to the heaviest known. In this case first-forbidden transitions, as given by the statistical gross theory, are taken into account.

error factor. The spread σ_{r_1} can be expected to be related to uncertainties in the positions of the levels in the underlying single-particle model. The use of a logarithm in the definition of r_1 implies that these two quantities correspond directly to distances as seen by the eye in, for example, Fig. 4, in units where one order of magnitude is 1. After the error analysis has been carried out we want to discuss its result in terms like "on the average the calculated half-lives are 'a factor of two' too long." To be able to do this we must convert back from the logarithmic scale. Thus, we realize that the quantities $M_{r_1}^{10}$ and $\sigma_{r_1}^{10}$ are conversions back to "factor of" units of the quantities M_{r_1} and σ_{r_1}, which are expressed in distance or logarithmic units.

We are now in a position to analyze the deviations between or calculations and experiment. An analysis of the half-life comparisons in Fig. 4 is given in Table 1 and of the β-delayed neutron-emission probability comparisons in Fig. 5 in Table 2. The half-life comparison shows, as earlier [6, 7] that the mean deviation of the calculated half-lives from the experimental values is approximately zero, that is $M_{r_1} \approx 0$. Thus, no "renormalization" of the calculated β-strength is indicated. This is true both for the GT calculation, and in particular for the GT+*ff* calculation. The large mean error for the GT calculation that is obtained when nuclei with very long half-lives are included do not indicate a need for a general renormalization, then the same renormalization should have been needed for nuclei with short half-lives and it is not. Rather the increase of the mean error in the GT calculation as the half-lives become longer arises because the effect of *ff* strength is not considered in the half-life calculation. When the *ff* strength is included in the half-life calculation the mean deviation is always very close to zero. In addition, in the GT+*ff* case the total error factor $\Sigma_{r_1}^{10}$ increases only very slowly when nuclei with very long half-lives are included in the calculations. This increase is expected because when the Q_β window

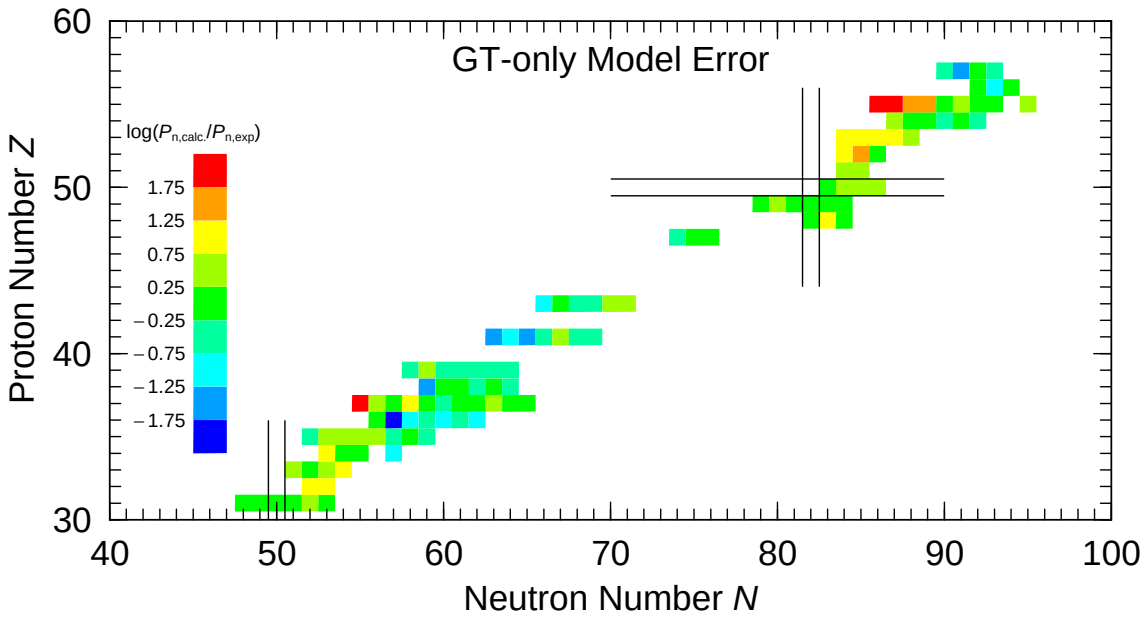

Figure 8: "Nuclear-chart" plot of the ratio of calculated to experimental β^--delayed neutron-emission probabilities for nuclei in the fission-fragment region.

becomes increasingly small the calculated half-life values are more sensitive to small errors in the calculated positions in energy of the GT transitions.

For delayed-neutron emission there is less data available than for β-decay half-lives. However,

Table 1: Analysis of the discrepancy between calculated and measured β^--decay half-lives shown in Fig. 4.

Model	n	M_{r_1}	$M^{10}_{r_1}$	σ_{r_1}	$\sigma^{10}_{r_1}$	Σ_{r_1}	$\Sigma^{10}_{r_1}$	$T^{\max}_{\beta,\exp}$ (s)
GT	546	0.34	2.20	1.28	19.09	1.33	21.17	1000.0
GT + *ff*	546	-0.04	0.92	0.68	4.81	0.68	4.82	1000.0
GT	431	0.19	1.55	0.94	8.81	0.96	9.21	100.0
GT + *ff*	431	-0.04	0.91	0.61	4.10	0.61	4.12	100.0
GT	306	0.14	1.38	0.77	5.87	0.78	6.04	10.0
GT + *ff*	306	-0.03	0.93	0.55	3.52	0.55	3.53	10.0
GT	184	0.03	1.06	0.57	3.72	0.57	3.73	1.0
GT + *ff*	184	-0.08	0.84	0.48	3.04	0.49	3.08	1.0
GT	137	-0.01	0.97	0.55	3.53	0.55	3.53	0.5
GT + *ff*	137	-0.09	0.81	0.49	3.10	0.50	3.17	0.5
GT	72	-0.04	0.92	0.54	3.44	0.54	3.45	0.2
GT + *ff*	72	-0.10	0.80	0.50	3.19	0.51	3.25	0.2
GT	42	-0.03	0.94	0.51	3.24	0.51	3.25	0.1
GT + *ff*	42	-0.08	0.83	0.47	2.92	0.47	2.97	0.1

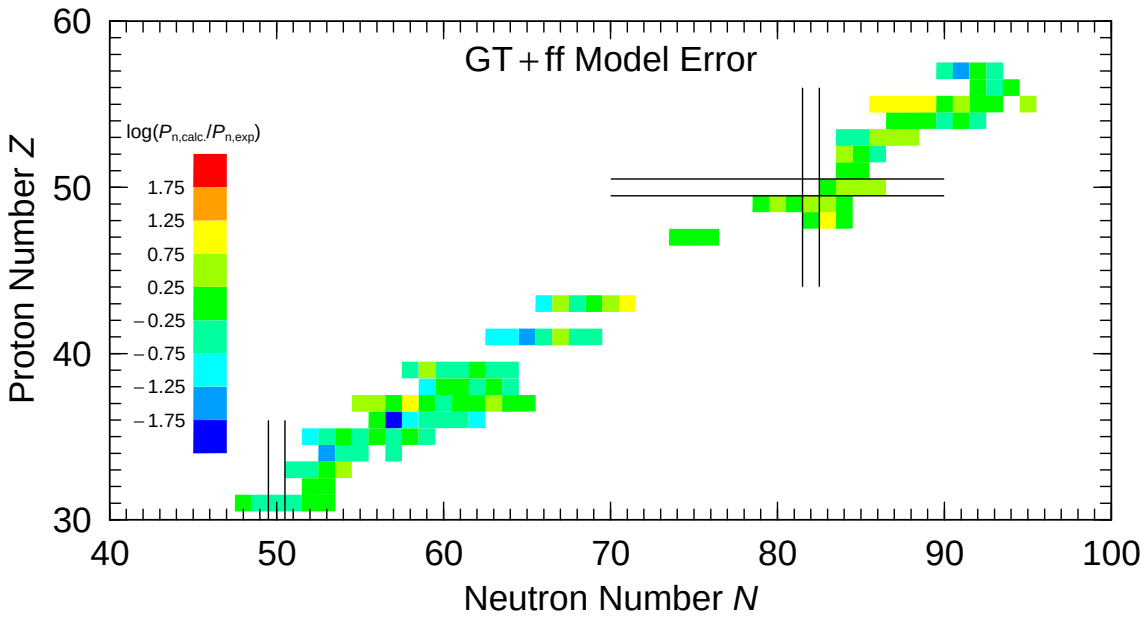

Figure 9: "Nuclear-chart" plot of the ratio of calculated to experimental β^--delayed neutron-emission probabilities for nuclei in the fission-fragment region. In this case first-forbidden transitions, as given by the statistical gross theory, are taken into account.

the number of data points are sufficient to allow us to draw several conclusions. First, just as for the half-lives we find that the calculations are more accurate for decays corresponding to large Q_β values, that is far from stability where data are often not available. Large Q_β values usually correspond to large P_n values. Second, we find also here that including *ff* transitions in the simple statistical gross theory model considerably improves the calculations.

To gain further insight into the consequences of including *ff* transitions in our β-strength functions we make several comparisons. In Figs. 6 and 7 we plot $\log(T_\mathrm{calc}/T_\mathrm{exp}$ for calculations without and with *ff* strength included in "nuclear chart" form. The results without *ff* transitions

Table 2: Analysis of the discrepancy between calculated and measured β-delayed neutron-emission probabilities P_n values shown in Fig. 5.

Model	n	M_{r_1}	$M^{10}_{r_1}$	σ_{r_1}	$\sigma^{10}_{r_1}$	Σ_{r_1}	$\Sigma^{10}_{r_1}$	$T^{\max}_{\beta,\mathrm{exp}}$ (s)
GT	126	0.08	1.21	0.74	5.48	0.74	5.54	100.0
GT + *ff*	126	-0.11	0.78	0.54	3.44	0.55	3.52	100.0
GT	74	0.04	1.10	0.75	5.66	0.74	5.50	10.0
GT + *ff*	81	-0.14	0.72	0.56	3.67	0.61	4.06	10.0
GT	43	0.06	1.16	0.75	5.66	0.71	5.18	1.0
GT + *ff*	43	-0.14	0.73	0.65	4.45	0.71	5.17	1.0
GT	16	0.18	1.52	1.08	11.94	0.94	8.80	0.1
GT + *ff*	19	-0.07	0.86	0.81	6.51	0.85	7.05	0.1

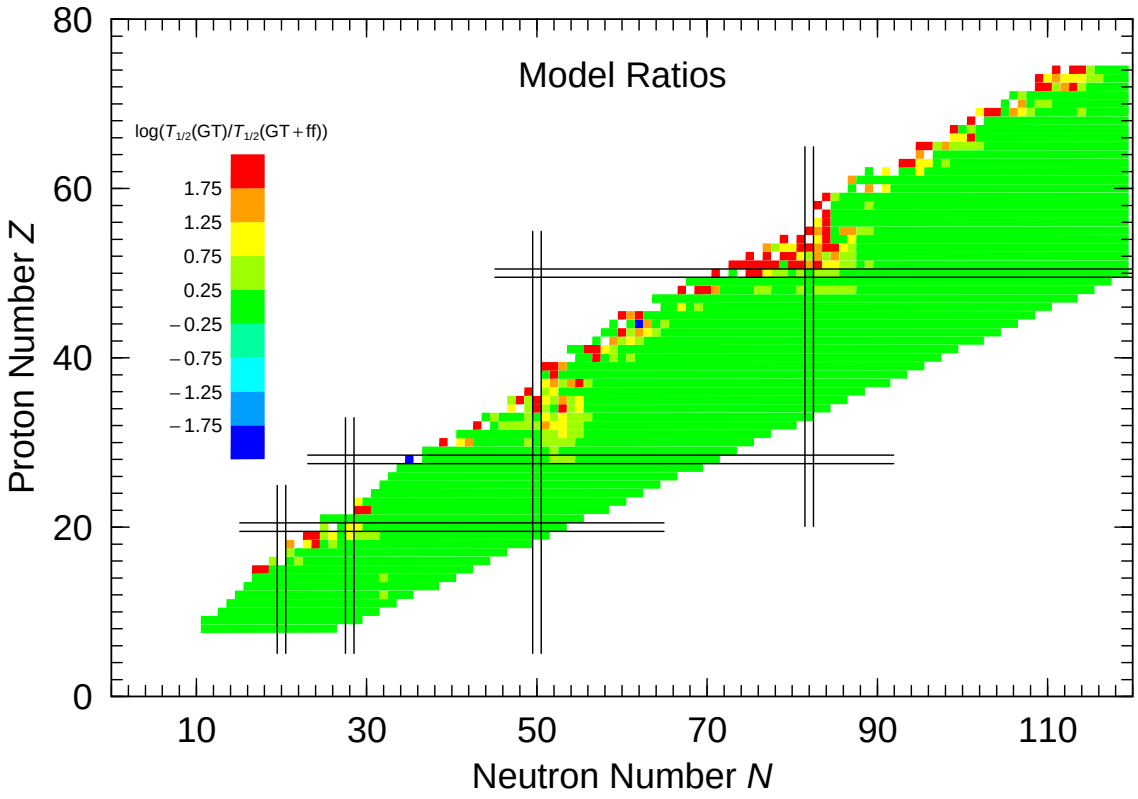

Figure 10: "Nuclear-chart" plot of the ratio of calculated β^--decay half-lives without and with first-forbidden transitions included. Just beyond $N = 50$ and $N = 82$ there is a significant decrease of the calculated half-lives in the r-process path when *ff* transitions are included.

in Fig. **??** are very clear: close to stability, and close to magic numbers the calculated half-lives are systematically much too long. The calculated half-lives are large near magic numbers also far from stability. This is very undesirable, the consequence will be that the calculated time for the r-process to reach the heavy region and to reach a steady-state situation can be expected to be too long compared to the actual duration. The reason for these deviations near β-stability and near magic numbers were elaborated on in our discussion above of Figs. 2 and 3. Figure 7 shows that when *ff* transitions are included then these systematic deviations largely dissappear. The behavior of calculated $P_{\rm n}$ values, shown in Figs. 8 and 9 is similar. We have substantially fewer data points here, but it is clear that some systematic deviations near β stability dissappear when *ff* transitions are included. In Fig. 10 we plot the ratio of the half-lives calculated without and with *ff* transitions included. As could be partly concluded already from our discussion of Figs. 6 and 7 we find big differences near β-stability and near magic numbers, in this latter case also far from stability. The differences are particularly noticeable just beyond $N = 50$ and $N = 82$ for nuclei in the vicinity of the r-process line. Above we made the case that the enhanced model with the *ff* transitions included is the more realistic one.

4 Speeding up the r-process

In order to study the effect of the new theoretical β-decay properties on r-process calculations to reproduce the solar-system isotopic r-abundance pattern ($N_{r,\odot}$), we use an extension of the classical "waiting-point" model as outlined in detail in Refs. [2, 34]. In our present time-dependent

calculations we use a superposition of 16 r-components with constant neutron densities in the range $10^{20} \leq n_{\rm n}[{\rm cm}^{-3}] \leq 3 \times 10^{27}$ and a constant (freeze-out) temperature $T_9 = 1.35$ (where T_9 is in units of 10^9 K) over varying process duration times τ_r. An instantaneous freeze-out of the initial "unprocessed r-progenitor distribution" was assumed. However, β-delayed emission of from one to three neutrons occurring during decay back to stability has fully been taken into account using our recent compilation of experimental $P_{\rm n}$ values [35, 36] together with theoretical predictions from either Ref. [7] ($P_{\rm n}$(GT)) or the present work ($P_{\rm n}$(GT+*ff*)).

Since occasionally questions arise concerning our interpretation of how in a simplified r-process model the observed r-abundance features and nuclear-physics properties far from stability are related, we summarize our main arguments once again. Initially, based on the identification of the first two classical neutron-magic waiting-point isotopes ^{80}Zn and ^{130}Cd [37–39] we have determined the $n_{\rm n}$–T_9 conditions of an r-process required to form the $A \simeq 80$ and 130 $N_{r,\odot}$ peaks at the right position (see, e.g. Figures 4 and 12 in Ref. [2] or Fig. 4 in Ref. [40]. Soon after, Takahashi et al. [41] have performed fully-dynamic r-process nucleosynthesis calculations within the realistic neutrino-wind model of a core-collapse supernova of type II (SN II). One of their promising results was that their time-varying trajectories of neutron densities (or entropies) and temperatures towards freeze-out were exactly lying within our predicted $n_{\rm n}$–T_9 band, thus proving the principal validity of our simple and elegant approximation.

The other issues addressed in detail following the above initial results were (i) what additional effects can enter in the "early" phases of an r-process (prior to freeze-out), and (ii) how can an astrophysically realistic treatment of a freeze-out alter the obtained r-abundance distribution. A summary of these discussions is given in the paper of Freiburghaus et al. [42]. It was agreed that, while heavy-element production in a realistic astrophysical scenario may well be fast in the very early phase with a r-process path close to the neutron drip-line, it is the final freeze-out with a path closer to β-stability (but still 15 to 35 mass-units away from it) that leaves its fingerprint in the observed $N_{r,\odot}$ pattern. Thus, at freeze-out the r-process seems to have "forgotten" his early history, and nuclear-structure effects of nuclei with $S_{\rm n} \simeq 1.5$–3 MeV — in particular at the magic neutron shells — determine the final picture. With respect to a realistic treatment of the freeze-out, several effects have been discussed, such as non-equilibrium captures of remaining seed neutrons and their inverse photo-disintegrations, re-capture of neutrons emitted after β-decay, and neutrino reactions. Detailed freeze-out tests have, however, shown that these effects do not affect the medium-heavy nuclei up to the $A \simeq 130$ $N_{r,\odot}$ peak significantly. But – somewhat depending on the specific astrophysical model – they may be important for the heavier nuclides in the rare-earth and the $A \simeq 195$ $N_{r,\odot}$ regions, although not changing the overall gross picture.

In summary, we can conclude that despite the above details, our admittedly rather simple and site-independent multicomponent model is a valuable approximation to the still favorably discussed realistic neutrino-wind scenario of a core-collapse SN II, well emulating the conditions just before and at freeze-out. Therefore, the waiting-point approximation has remained an important test-bed for systematic parameter studies of various nuclear data sets for masses and β-decay properties [34, 43–46].

In the context of this paper, the β-decay half-lives of the r-process progenitor isotopes are of major importance since they define to a large extent the time behavior of the r-process matter flow from the seed region (here assumed to be Fe) up to the Th, U and the $A \geq 250$ fission region. Thus, the half-lives determine the total duration of an r-process. In particular the rapidly expanding high-entropy bubble of the neutrino-wind SN II scenario would require a rather short r-process time scale of the order of 1 s. Under typical freeze-out conditions ($T_9 \simeq 1.35$ is chosen here) and with an Fe-group seed, this can only be achieved with "short" $T_{1/2}$. This is particularly the case for the classical $N = 50$, 82 and 126 waiting-point nuclei where the r-process *"climbs a staircase with Z and A both increasing by unity after each step"* when plotted versus mass number A [1], or it climbs a ladder at the magic shell when plotting versus neutron number

Table 3: Comparison of β-decay half-lives of neutron-magic $N = 50$, 82 and 126 r-process waiting-point nuclei from different tabulations. In column 2, we list the theoretical $T_{1/2}$ values for pure GT-decay [7]. Column 3 summarizes the corresponding values from our new $T_{1/2}$(GT+ff) calculations. And in column 4, we give our experimental values together with the (steadily updated) $T_{1/2}$ evaluation [35, 36] which we have used so far in most of our r-process calculations since the early 1990's [2].

Waiting-point Isotope	Beta-decay half-life [ms] $T_{1/2}$(GT)	$T_{1/2}$(GT+*ff*)	$T_{1/2}$(eval)
^{76}Fe	44.6	27.2	13.2
^{77}Co	13.4	13.7	9.8
^{78}Ni	477.1	224.4	210.0
^{79}Cu	430.3	156.8	188 *)
^{80}Zn	3068	1260	540 *)
^{81}Ga	1568	1227	1222 *)
^{125}Tc	9.1	8.9	7.5
^{126}Ru	34.2	29.7	16.6
^{127}Rh	22.0	20.4	69.7
^{128}Pd	125.1	74.2	115.0
^{129}Ag	47.0	31.7	46 *)
^{130}Cd	1123.1	502.3	168 *)
^{131}In	147.1	139.2	278 *)
^{190}Gd	14.2	9.4	15.8
^{191}Tb	15.9	10.2	13.8
^{192}Dy	31.6	19.7	30.0
^{193}Ho	27.7	17.7	20.4
^{194}Er	87.1	50.2	95.8
^{195}Tm	67.3	42.0	90.4
^{196}Yb	396.6	181.2	222.0

*) experimental value

N [47, 48]. At these magic neutron numbers, the r-process isotopes have the longest half-lives (the most important ones at $N \simeq 50$ and 82 have now been determined experimentally, cf. Refs. [19, 34, 37–39, 46, 49–51]. Thus, they form the major bottle necks for the r-matter flow at the rising wings of the $N_{r,\odot}$ peaks at $A \simeq 80$, 130 and 195.

Table 3 compares the $T_{1/2}$(GT) [7] with our new $T_{1/2}$(GT+*ff*) and with the (steadily updated) $T_{1/2}$ evaluation [35, 36] used in most of our r-process nucleosynthesis calculations since the early 1990's [2]. More than 40 years ago B^{2}FH [1] and Coryell [52] suggested that the sum of the half-lives of all r-process isotopes between Fe and the heaviest species in the Th, U region (in particular the "long" ones of the neutron-magic waiting-point nuclei at $N = 50$, 82 and 126) will yield a rough estimate of the total duration of an r-process (τ_r). When we follow this prescription it immediately becomes evident that our improved macroscopic-microscopic $T_{1/2}$(GT+*ff*) predictions, together with the known experimental data, will speed up the classical r-process considerably. Within this picture, clearly the $N = 50$ shell closure represents the strongest bottle-neck for the r-matter flow due to the rather long half-lives of ^{80}Zn and ^{81}Ga. Based on the theoretical $T_{1/2}$(GT) from Ref. [7], an r-process would need about 5.6 s to pass the $N = 50$ shell. With our new $T_{1/2}$(GT+*ff*) values this time would already be reduced to 2.9 s. When we take into account the measured half-lives for ^{79}Cu, ^{80}Zn and ^{81}Ga, the time duration further reduces to 1.2 s. Similarly, but not as strongly halted as at $N = 50$, the $N = 82$ shell

would be overcome within 1.5 s when using the $T_{1/2}$(GT) half-lives, speeded up to 0.8 s with the new $T_{1/2}$(GT+*ff*) half-lives, and reduced further to about 0.6 s when the experimental half-lives for ^{129}Ag, ^{130}Cd and ^{131}In are used. The waiting-point effect is somewhat less pronounced for the $N = 126$ shell, where no experimental data are now available nor can be expected to be available in the near future. When we sum up the theoretical half-lives of the neutron-magic r-process nuclei between ^{190}Gd and ^{196}Yb, the use of our $T_{1/2}$ evaluation [35, 36] yields a value of 0.49 s, to be compared to 0.64 s for the $T_{1/2}$(GT) from [7] and 0.33 s for the new $T_{1/2}$(GT+*ff*). In summary, most of the time needed for an r-process is to overcome the $N = 50$ and $N = 82$ bottle-neck regions, whereas the N=126 shell is passed relatively quickly. As soon as the r-process succeeds to break out of the magic neutron shells at ^{81}Ga, ^{131}In and ^{196}Yb, respectively, the matter flow will accelerate in the regions in between the abundance peaks and beyond $A \simeq 200$. In these regions mainly very short-lived deformed r-process progenitors are involved. For these the earlier $T_{1/2}$(GT) [7] are quite similar to our new $T_{1/2}$(GT+*ff*) predictions.

Today we know, however, that the initial picture of B^{2}FH [1] of summing-up the $T_{1/2}$ of the waiting-point nuclei of all three magic shells $N = 50$, 82 and 126 is too simplistic, and in fact not quite correct. Since the early 1990's, at the latest, when the first experimental information about the r-process isotopes ^{80}Zn and ^{130}Cd became available, it is definitely clear that the formation of the three $N_{\mathrm{r},\odot}$ peaks requires different neutron-density conditions, implying different r-process paths at different distances from β-stability [2, 43, 48]. To be more specific, under the astrophysical n_{n}–τ_{r} conditions where the $A \simeq 80$ peak is produced at relatively "low" n_{n}, the $A \simeq 130$ peak will barely be formed and definitely not the $A \simeq 195$ peak, unless "higher" n_{n} densities are invoked. Similarly, for n_{n}–τ_{r} conditions where the $A \simeq 130$ peak is produced at "medium" n_{n} densities (see, e.g. Fig. 11 of this paper), the $A \simeq 80$ region has already been partly depleted, and the $A \simeq 195$ peak only starts to fill up. Hence, at least three n_{n}-components are required with - consequently - shorter process durations τ_{r} to model the respective mass regions. This is demonstrated, in, for example, Figures 3 and 5 of Ref. [38]. Even within each series of neutron-magic isotones, the respective r-process isotopes act as waiting-points for different n_{n}-ranges.

Let us have a closer look into the situation at the 2nd $N_{\mathrm{r},\odot}$ peak involving the $N = 82$ waiting-point nuclei ^{127}Rh to ^{131}In. For $n_{\mathrm{n}} \simeq 2 \times 10^{22}$ [cm^{-3}] the r-process breaks out of the magic shell at ^{131}In. Under these conditions, the $N = 50$ isotopes ^{77}Co to ^{79}Cu would still lie in the r-process path; but above $Z = 29$ the waiting-point nuclei would be $N = 52$ ^{82}Zn and $N = 84$ ^{85}Ga. In terms of the τ_{r} of this r-component, this means that the matter flow avoids the two relatively "long-lived" waiting points ^{80}Zn ($T_{1/2} = 540$ ms) and ^{81}Ga ($T_{1/2} = 1.2$ s) and speeds up through the above "shorter-lived" r-process nuclei with $T_{1/2}(\mathrm{GT} + \mathrm{ff}) = 275$ ms and 268 ms, respectively. At $n_{\mathrm{n}} \simeq 5 \times 10^{23}$ [cm^{-3}] the r-process breaks out of $N = 82$ already in the Cd chain, thus avoiding the 168-ms ^{130}Cd in favor of 97-ms ^{132}Cd. Analogously, below $Z = 48$ ^{129}Ag acts as a neutron-magic waiting-point nucleus up to $n_{\mathrm{n}} \simeq 5 \times 10^{24}$ [cm^{-3}] (with ^{132}Cd and ^{135}In for $Z = 48$ and 49), ^{128}Pd up to $n_{\mathrm{n}} \simeq 10^{26}$ [cm^{-3}] (now with ^{131}Ag, ^{134}Cd and ^{137}In above $Z = 46$) and ^{127}Rh up to $n_{\mathrm{n}} \simeq 3 \times 10^{27}$ [cm^{-3}] (with ^{130}Pd, ^{133}Ag, ^{136}Cd and ^{139}In above $Z = 45$). Under the latter n_{n}-conditions, already the 3rd $N_{\mathrm{r},\odot}$ peak at $A \simeq 195$ is formed. Break-out from the $N = 126$ shell closure at ^{195}Tm occurs at $n_{\mathrm{n}} \simeq 2 \times 10^{27}$. At such high neutron densities, the r-process would already break out of the $N = 50$ shell at $Z = 28$ (thus "saving" nearly 2 s at the $A \simeq 80$ bottle-neck; see Table 3), and out of the $N = 82$ shell at $Z = 128$ (thus "saving" another 500 ms at the $A \simeq 130$ bottle-neck). All these above considerations about the r-process paths and the corresponding τ_{r} are, however, still based on simple static calculations using the nuclear Saha equation. A more realistic picture will, therefore, only be obtained through time-dependent r-process calculations. Therefore, our next step will be to investigate the r-process matter flow in a dynamic model with the classical (n,γ)$\rightleftharpoons$ (γ,n) equilibrium assumption (see, e.g. Refs. [2, 34]).

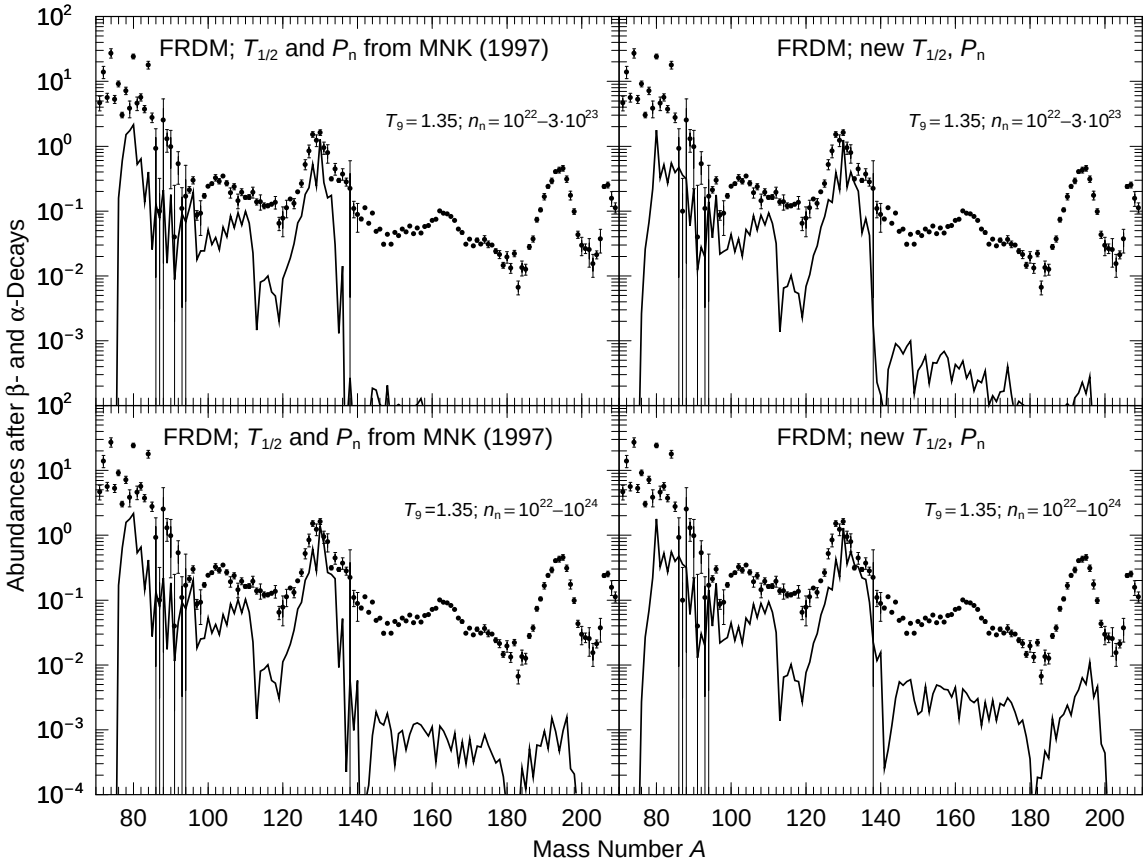

Figure 11: Comparison of calculated r-abundance n_n–τ_r components which mainly build the A≃130 $N_{r,\odot}$ peak at a freeze-out temperature of $T_9 = 1.35$, using exclusively theoretical $T_{1/2}$(GT) and P_n(GT) values from Ref. [7] (left part) with our new $T_{1/2}$(GT+*ff*) and P_n(GT+*ff*) predictions (right part). In all calculations, nuclear masses were used from the Audi evaluation [33] or from the FRDM model [4]. It is clearly evident from this comparison, that – within the same process times $\tau_r = 2.00$ s for the upper figures and $\tau_r = 2.15$ s – the shorter $T_{1/2}$(GT+*ff*) result in a faster r-matter flow at the $N = 82$ bottle-neck region, thus producing already considerably higher r-abundances of rare-earth elements than with the use of the older $T_{1/2}$(GT) values. For more details, see text.

To show the situation in more detail, Fig. 11 compares snapshots of time-dependent r-abundance calculations for a range of astrophysical conditions (with identical T_9, n_n and τ_r, respectively) under which the second $N_{r,\odot}$ peak at $A \simeq 130$ is formed. Together with the neutron separation energies from the FRDM mass model [4], the $T_{1/2}$ and P_n values become the decisive nuclear quantities in these calculations. And, as is clearly evident from the figure, with our new, "shorter" $T_{1/2}$(GT+*ff*) at the same process time considerably more r-material has been built up beyond the peak in the rare-earth region than with our old, "longer" $T_{1/2}$(GT).

Finally, Fig. 12 shows the development of the r-abundances of the important waiting-point isotopes ^{80}Zn ($N = 50$), ^{130}Cd ($N = 82$) and ^{195}Tm (N=126) as a function of neutron density n_n and process duration τ_r, respectively. These three nuclei form the respective top of the three $N_{r,\odot}$ peaks at freeze-out prior β-decay back to stability. Again, one observes that the new macroscopic-microscopic $T_{1/2}$(GT+*ff*) predictions result in a speeding-up of the r-process compared to the earlier half-lives for pure GT-decay [7]. With this, the total duration for a robust r-process nucleosynthesis up to Th, U is reduced to about 4 s. This is slightly more than the time scale we had obtained already 10 years ago with our $T_{1/2}$ and P_n evaluation [35, 36], which

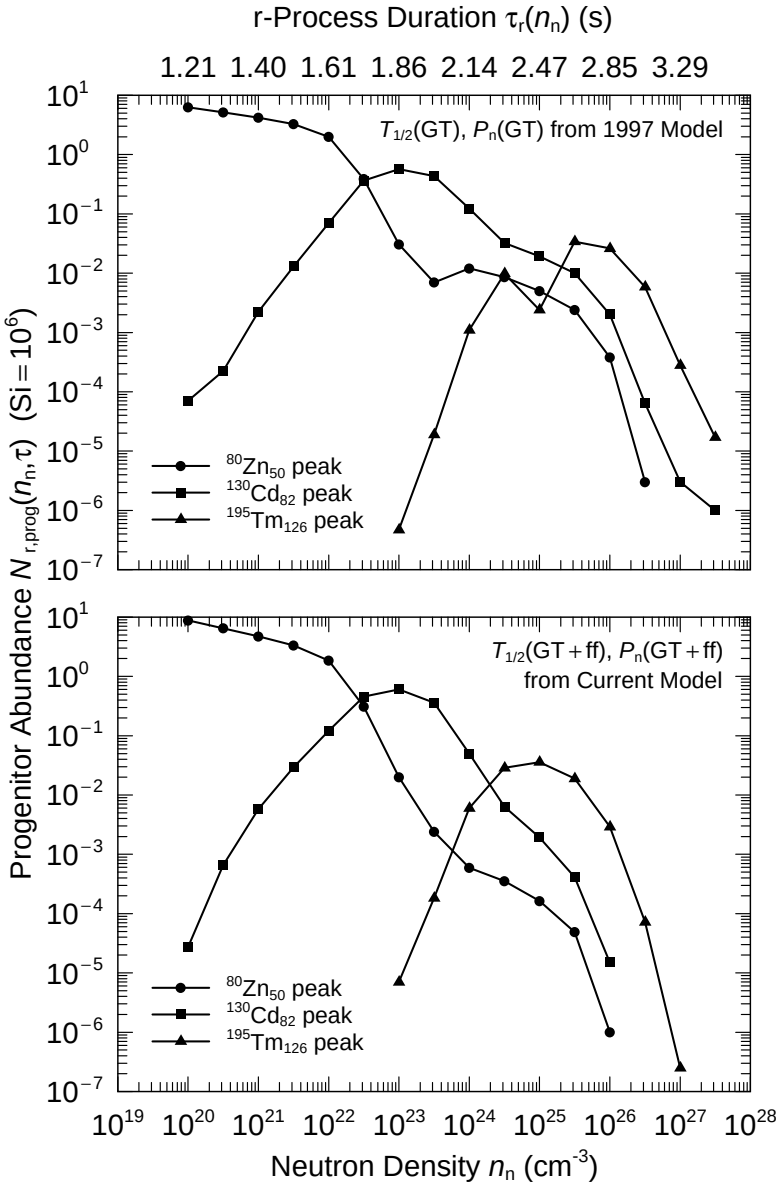

Figure 12: The build-up of the initial r-abundances $N_{r,\mathrm{prog}}$ of the three neutron-magic waiting-point nuclides ^{80}Zn$_{50}$, ^{130}Cd$_{82}$ and ^{195}Tm$_{126}$ from an Fe-seed as a function of neutron density n_{n} and process duration τ_r at freeze-out temperature $T_9 = 1.35$. The above three isotopes are the direct progenitors of the stable isobars ^{80}Se, ^{130}Te and ^{195}Pt situated at the top of the respective $N_{r,\odot}$ peaks. Their build-up contains the full time-history of the r-process "climbing up" the respective magic neutron shells at $N = 50$, 82 and 126. Furthermore, in the formation of the 2nd and 3rd $N_{r,\odot}$ peaks, a kind of "memory effect" of the history of the r-matter flow at the earlier r-peak(s) is maintained. The upper part shows the calculations using the β-decay half-lives $T_{1/2}$(GT) obtained from the QRPA model for GT-decay only [6]. The lower part exhibits the respective calculations using our new, shorter theoretical $T_{1/2}$(GT+*ff*) values which include both GT-decay (from the QRPA model) and *ff*-decay (from the "gross theory" [23]). In all calculations, nuclear masses have consistently been taken from the most recent Audi evaluation [33] and from the FRDM model [4].

included experimental data and local nuclear-structure related improvements in the theoretical calculations of β-decay properties, as outlined e.g. in Ref. [2].

In this paper, we have for consistency reasons based all our calculations on the FRDM mass model [4], in which neutron-shell corrections in the vicinity of magic neutron numbers far from

stability, in particularly in the waiting-point regions, are sometimes as strong as the experimentally known ones in the valley of β-stability. This model currently presents the most well-tested and most unified prescription for obtaining unknown nuclear properties far from stability, with the best, proven track record of reliability for a large number of nuclear-structure properties, when calculated quantities are compared to new data as they become available [7]. However, it is informative to investigate the consequences of slightly more speculative assumptions. Recent experimental evidence is often interpreted to indicate that a gradual shell weakening ("quenching") of the classical shell gaps with distance from stability — already well known for $N = 20$ and $N = 28$ — also seems to occur at $N = 50$ and $N = 82$. For recent reviews, see for example Refs. [34, 46]. Such a weakening of the shell effects may further speed up the classical r-process even at moderate neutron densities. In a calculation based on, for example, the microscopic Hartree-Fock-Bogolyubov (HFB) method with the specific Skyrme force SkP of Dobaczewski et al. [53, 54], which exhibits a rather strong shell quenching, a robust r-process from the classical Fe seed up to the full 3rd $N_{r,\odot}$ peak can be run within about 1.5 s with a maximum neutron density of only $n_{\rm n} \simeq 10^{23}[{\rm cm}^{-3}]$ (see, e.g. Fig. 3 in Ref. [43] or Fig. 4 in Ref. [46]. However, in for example the neutrino-wind SN II scenario, the rapid-neutron-capture process starts from an $A \simeq 90$ seed composition, and consequently it avoids the dominant $N = 50$ bottle-neck in the r-matter flow. In this scenario, with a calculation based on the "quenched-shell" assumption, the total duration of an r-process at freeze-out can be further reduced to about 850 ms.

It will presumably not be a problem to obtain short half-lives of r-process progenitor nuclei and corresponding short time-scales to build up heavy elements in low-entropy environments which are very neutron-rich, such as neutron-star (NS) mergers [55–57] but it is still a difficult problem to realize short progenitor half-lives in high-entropy environments with (only) moderate neutron densities, such as SN II scenarios. As shown, by for example Refs. [42, 58], rather high entropies up to 400 $k_{\rm B}$/nucleon are required to produce the full 3rd $N_{r,\odot}$ peak at $A \simeq 195$. Such high densities are considerably beyond what is achieved in realistic hydrodynamic approaches [41, 59]. However, if shell quenching at $N = 50$ and 82 would definitely be confirmed by future experiments, the above maximum neutron density of roughly $10^{23}[{\rm cm}^{-3}]$ – which would correspond to a maximum entropy of about 150 $k_{\rm B}$/nucleon – together with an r-process timescale of the order of 1 s might help to solve at least some of the still existing problems encountered in the high-entropy neutrino-wind SN II scenario.

A sentence added: Even if time-scales should turn out to be of minor importance in realistic r-process nucleosynthesis scenarios, we prefer to use the best possible (experimental and consistently calculated microscopic) nuclear-data input in our calculations, rather than compensating obvious nuclear-physics deficiencies by "optimizing" simultaneously several (not so well defined) astrophysical quantities as "free parameters".

5 Summary and conclusions

We have combined our microscopic QRPA model of allowed Gamow-Teller β decay with the statistical gross theory of first-forbidden decay. Experimental data show that the first-forbidden strength over a given energy range is represented by numerous densely spaced peaks whereas the allowed GT strength is concentrated in a few strong peaks. Our new "microscopic-macroscopic" model of β decay is therefore a reasonable approximation in analogy with the microscopic-macroscopic model of nuclear potential-energy surfaces. It is also the, at the moment, only tractable way to calculate globally the required nuclear-structure and decay properties in a model that represents a unified model across the entire nuclear chart and that has a proven track record of reliability when it is applied far from known regions of nuclei where the model parameters were determined [4, 7]. We have tested our approach by comparing the new model and old model, the latter without first-forbidden decays taken into account, to data throughout the periodic system.

These comparisons demonstrated that our enhanced model leads to a substantial improvement in calculated β-decay half-lives and β-delayed neutron-emission probabilities. This is particularly true near magic neutron numbers where the r-process "spends most of its time."

The new $T_{1/2}$(GT+*ff*) and $P_{\rm n}$(GT+*ff*) values have been applied to site-independent r-process calculations. Calculations based on the new data base result in a considerable speeding-up of the r-matter flow in the vicinity of the $N_{r,\odot}$ peaks, which are related to magic neutron-shell closures, relative to calculations based on the previous $T_{1/2}$(GT) and $P_{\rm n}$(GT) tabulation.

Clearly, still more work is needed in both experimental and theoretical nuclear physics as well as in astrophysics to finally solve the problem of the *"origin of the heavy elements between Fe and Th, U"* which has recently been considered number three among "The 11 Greatest Unanswered Questions in Physics" [60].

Acknowledgments

This work was supported by the U. S. Department of Energy, the German Bundesministerium für Bildung und Forschung, and Gesellschaft für Schwerionenforschung.

References

[1] E. M. Burbidge, G. R. Burbidge, W. A. Fowler, and F. Hoyle, Rev. Mod. Phys. **29** (1957) 547.

[2] K.-L. Kratz, J.-P. Bitouzet, F.-K. Thielemann, P. Möller, and B. Pfeiffer, Astrophys. J. **403** (1993) 216.

[3] P. Möller and J. R. Nix, Atomic Data Nucl. Data Tables **26** (1981) 165.

[4] P. Möller, J. R. Nix, W. D. Myers, and W. J. Swiatecki, Atomic Data Nucl. Data Tables **59** (1995) 185.

[5] J. Krumlinde and P. Möller, Nucl. Phys. **A417** (1984) 419.

[6] P. Möller and J. Randrup, Nucl. Phys. **A514** (1990) 1.

[7] P. Möller, J. R. Nix, and K.-L. Kratz, Atomic Data Nucl. Data Tables **66** (1997) 131.

[8] P. A. Seeger and W. M. Howard, Nucl. Phys. **A238** (1975) 491.

[9] Y. Aboussir, J. M. Pearson, A. K. Dutta, and F. Tondeur, Atomic Data Nucl. Data Tables **61** (1995) 127.

[10] J. M. Pearson, R. C. Nayak, and S. Goriely, Phys. Lett B **387** (1996) 455; and ETFSI-Q Mass Table, priv. comm.

[11] S. Goriely, F. Tondeur, and J. M. Pearson, At. Data Nucl Data Tables, **77** (2001) 311.

[12] O. Bohigas and P. Lebœuf, Phys. Rev. Lett. **8809** (2002) 2502.

[13] O. Bohigas and P. Lebœuf, Phys. Rev. Lett. **8812** (2002) 9903.

[14] C. L. Duke, P. G. Hansen, O. B. Nielsen, and G. Rudstam, Nucl. Phys. **A151**, (1970) 609.

[15] T. Tachibana, H. Nakata, and M. Yamada, AIP Conf. Proc. **425** (1998) 495.

[16] K.-L. Kratz, Nucl. Phys. **A417** (1984) 447.

[17] O. Sorlin, D. Guillemaud-Mueller, A. C. Müller, V. Borrel, S. Dogny, F. Pougheon, K.-L. Kratz, H. Gabelmann, B. Pfeiffer, A. Wöhr, W. Ziegert, Y. E. Penionzhkevich, S. M. Lukyanov, V. S. Salamatin, R. Anne, C. Borcea, L. K. Fifield, M. Lewitowicz, M. G. Saint-Laurent, D. Bazin, C. Détraz, F.-K. Thielemann, and W. Hillebrandt, Phys.Rev.C **47** (1993) 2941.

[18] K.-L. Kratz, P. Möller, and W. B. Walters, Proc. Tenth International Symposium on Capture Gamma-Ray Spectroscopy and Related Topics, Santa Fe, New Mexico, USA, August 30 - September 3, 1999 (AIP Conf. Proc. **529** (2000) 295).

[19] M. Hannawald, K. L. Kratz, B. Pfeiffer, W. B. Walters, V. N. Fedoseyev, V. I. Mishin, W. F. Mueller, H. Schatz, J. VanRoosbroeck, U. Köster, V. Sebastian, H. L. Ravn, Phys. Rev. C **6205** (2000) 4301.

[20] A. Wöhr, A. Ostrowski, K.-L. Kratz, I. Dillmann, A.M. El-Taher, V. Fedoseyev, L. Fraile, H. Fynbö, U. Köster, B. Pfeiffer, H.L. Ravn, M. Seliverstov, J. Shergur, L. Weissman, W.B. Walters, and the ISOLDE Collaboration, Proc. 11th *Workshop on Nuclear Astrophysics*, Ringberg Castle, Lake Tegernsee, Germany, February 11–16, 2002 (Max-Planck-Institut für Astrophysik Report, MPA/P13 (2002) p. 79).

[21] K.-L. Kratz and G. Herrmann, Z. Physik **263** (1973) 435.

[22] K. Takahashi, Prog. Theoret. Phys. **47** (1972) 1500.

[23] K. Takahashi, M. Yamada, and T. Kondoh, Atomic Data Nucl. Data Tables **12** (1973) 101.

[24] I. N. Borzov, S. A. Fayans, E. Kromer, D. Zawischa, Z. Physik A **355** (1996) 117.

[25] M. Hirsch, A. Staudt, K. Muto, H. V. Klapdor-Kleingrothaus, At. Data Nucl. Data Tables, **53** (1993) 165.

[26] H. Homma, E. Bender, M. Hirsch, K. Muto, H. V. Klapdor-Kleingrothaus, T. Oda, Phys. Rev. C **54** (1996) 2972.

[27] I. Hamamoto, Nucl. Phys. **62** (1965) 49.

[28] J. A. Halbleib, Sr. and R. A. Sorensen, Nucl. Phys. **A98** (1967) 542.

[29] M. A. Preston, Physics of the nucleus (Addison-Wesley, Reading, 1962).

[30] N. B. Gove and M. J. Martin, Nucl. Data Tables **10** (1971) 205.

[31] A. deShalit and H. Feshbach, Theoretical physics, vol. I: Nuclear structure (Wiley, New York, 1974).

[32] G. Audi, Midstream atomic mass evaluation, private communication (1989), with four revisions.

[33] G. Audi and A. H. Wapstra, Nucl. Phys. **A595** (1995) 409.

[34] K.-L. Kratz, B. Pfeiffer, F.-K. Thielemann, W.B. Walters, Hyperfine Interactions, **129** (2000) 185.

[35] K.-L. Kratz, B. Pfeiffer and P. Möller, *Evaluation of* $T_{1/2}$ *and* P_{n} *values*, KCh Mainz Report, 1996 (unpublished) and
URL: www.kernchemie.uni-mainz.de/∼pfeiffer/khf/.

[36] B. Pfeiffer, K.-L. Kratz, and P. Möller, Prog. Nucl. Energy, in print.

[37] K.-L. Kratz, H. Gabelmann, W. Hillebrandt, B. Pfeiffer, K. Schlosser, F.-K. Thielemann, Zeit. Phys. **385** (1986) 489.

[38] B. Ekström, B. Fogelberg, P. Hoff, E. Lund, A. Sangariyavanish, Physica Scripta **34** (1986) 614.

[39] R.L. Gill, R.F. Casten, D.D. Warner, A. Piotrowski, H. Mach, J.C. Hill, F.K. Wohn, J.A. Winger, R. Moreh, Phys. Rev. Lett **56** (1986) 1874.

[40] K.-L. Kratz et al, Origin of the Elements in the Solar System: Implications of Post-1957 Observations, Kluwer/Plenum, New York (2001) 119.

[41] K. Takahashi, J. Witti, and H.-T. Janka, Astron. Astrophys. **286** (1994) 857.

[42] C. Freiburghaus, J.F. Rembges, T. Rauscher, E. Kolbe, F.-K. Thielemann, K.-L. Kratz, B. Pfeiffer, J.J. Cowan, Astrophys. J. **516** (1999) 381.

[43] K.-L. Kratz, B. Pfeiffer, F.-K. Thielemann Nucl. Phys. **A630** (1998) 352c.

[44] K.-L. Kratz, Nucl. Phys. **A688** (2001) 308c.

[45] B. Pfeiffer, K.-L. Kratz, F.-K. Thielemann, Z. Phys. **A357** (1997) 235.

[46] B. Pfeiffer, K.-L. Kratz, F.-K. Thielemann, W.B. Walters Nucl. Phys. **A693** (2001) 282.

[47] K.-L. Kratz, F.-K. Thielemann, W. Hillebrandt, P. Möller, V. Harms, A. Wöhr, and J. W. Truran, Proc. 6th Int. Symp. on capture gamma-ray spectroscopy, Leuven, 1987, Inst. Phys. Conf. Ser. No. **88**, J. Phys. G:Nucl. Phys. **14** Suppl. (1988) p. S331.

[48] K.-L. Kratz, Rev. Mod. Astron. **1** (1988) 184.

[49] K.-L. Kratz, H. Gabelmann, P. Möller, B. Pfeiffer, H.L Ravn, A. Wöhr, Z. Phys. **A340** (1994) 419.

[50] K.-L. Kratz, T. Kautzsch, M. Hannawald, W. Böhmer, I. Klöckl, P. Möller, and B. Pfeiffer, V. N. Fedoseyev, V. I. Mishin, W. B. Walters, A. Wöhr, P.van Duppen, Y, Jading, H. L. Ravn, J. Lettery, V. Sebastian, M. Koizumi, U. Köster, and the ISOLDE Collaboration, Proc. Int. Conf. on Fission and Properties of Neutron-Rich Nuclei, Ed. J. H. Hamilton and A. V. Ramayya, Sanibel Island, Florida, 10–15 November 1997, (World Scientific, Singapore, (1998) p. 586).

[51] K.-L. Kratz, Proc. ENAM 98, Exotic Nuclei and Atomic Masses, Bellaire, Michigan, 23–27 June, 1998 (AIP Conference Proceedings, **455** (1998) 827).

[52] C.D. Coryell, J. Chem. Educ. **38** (1961) 67.

[53] J. Dobaczewski, I. Hamamoto, W. Nazarewicz, and J. A. Sheikh, Phys. Rev. Lett. **72** (1994) 981.

[54] J. Dobaczewski, W. Nazarewicz, T. R. Werner, Phys. Scr. **T56** (1995) 15.

[55] J. M. Lattimer, F. Mackie, D. G. Ravenhall, D. N. Schramm Astrophys. J. **213** (1977) 225.

[56] S. Rosswog, M. Liebendorfer, F.-K. Thielemann, M.B. Davies, W. Benz, T. Piran, Astron. Astrophys. **341** (1999) 499.

[57] S. Rosswog, M.B. Davies, F.-K. Thielemann, T. Piran, Astron. Astrophys. **360** (2000) 171.

[58] S. E. Woosley, J.R. Wilson, G. J. Mathews, R.D. Hoffman, B. S. Meyer Astrophys. J. **433** (1994) 229.

[59] Y. Z. Qian and S. E. Woosley, Astrophys. J. **471** (1996) 331.

[60] E. Haseltine, Discover Magazine, **23**, No 2, February 2002.